A Journal of the Gesellschaft Deutscher Chemiker

Angewandte International Edition

GDCh

Chemie

www.angewandte.org

Accepted Article

Title: Exploiting Mechanistic Solvation Kinetics for Dual-Graphite Batteries with High Power Output at Extremely Low Temperature

Authors: John Holoubek, Yijie Yin, Mingqian Li, Mingyu Yu, Ying Shirley Meng, Ping Liu, and Zheng Chen

To be cited as: *Angew. Chem. Int. Ed.* 10.1002/anie.201912167
Angew. Chem. 10.1002/ange.201912167

Link to VoR: http://dx.doi.org/10.1002/anie.201912167
http://dx.doi.org/10.1002/ange.201912167

WILEY-VCH

10.1002/anie.201912167

Exploiting Mechanistic Solvation Kinetics for Dual-Graphite Batteries with High Power Output at Extremely Low Temperature

John Holoubek[a], Yijie Yin[c], Mingqian Li[b], Mingyu Yu[c], Ying Shirley Meng[a,c,d], Ping Liu[a,b,c,d]*, Zheng Chen[a,b,c,d]*

[a]*Department of NanoEngineering, University of California, San Diego, La Jolla, CA 92093, USA*

[b]*Program of Chemical Engineering, University of California, San Diego, La Jolla, CA 92093, USA*

[c]*Program of Materials Science, University of California, San Diego, La Jolla, CA 92093, USA*

[d]*Sustainable Power and Energy Center, University of California, San Diego, La Jolla, CA 92093, USA*

Abstract

Improving the extremely low temperature operation of rechargeable batteries is vital to the operation of electronics in extreme environments, where systems capable of high-rate discharge are in short supply. Herein, we demonstrate the holistic design of dual-graphite batteries, which circumvent the sluggish ion desolvation process found in typical lithium-ion batteries during discharge. These batteries were enabled by a novel electrolyte, which simultaneously provided high electrochemical stability and ionic conductivity at low temperature. The dual-graphite cells, when compared to industry-type graphite || $LiCoO_2$ full-cells demonstrated an 11 times increased capacity retention at -60 ºC for a 10 C discharge rate, indicative of the superior kinetics of the "dual-ion" storage mechanism. These trends are further supported by GITT and EIS measurements at reduced temperature. This work provides a new design strategy for extreme low-temperature batteries.

Introduction

The advent of lithium-ion batteries (LIBs) has enabled the rapid development of portable electronics and electric vehicles due to their relatively high specific energy and long cycle life under mild operating conditions.[1] However, typical LIBs encounter severe performance loss at sub-zero temperatures primarily due to the liquid electrolyte, which hinders the deployment of high altitude drones and advanced electronics in space.[2] In particular, power density suffers severely, where early studies observed that a commercial LIB retaining 5% of its energy density at -40ºC only retained 1.25 % of its power density.[3]

External battery warming systems are typically applied to circumvent this issue, where device charging in harsh environments can be aided by additional components that have recently been demonstrated with minimal impact to total cell mass.[4] However, these heating systems are untenable for discharge as a standalone system due to their non-negligible startup times, requiring a source of high current for initial activation. Furthermore, many devices requiring low temperature discharge do not require warming systems for charging due to the nature of their operation (e.g. high-altitude drones are charged at low altitudes). For these reasons, the field has traditionally focused on performance retention at low-temperature during discharge after charging under mild conditions.[2,3]

Approaches to improve low-temperature discharge performance generally focus on the battery electrolyte, which facilitates the transport of ions between electrodes and governs a set of discrete cell impedance contributors. For a typical discharging LIB, these contributions are generally summarized as: 1) migration through the solid-electrolyte-interface (SEI), 2) bulk ionic transport, and 3) charge-transfer, which is dominated by Li^+ de-solvation at the positive electrode interface.[5]

These resistances are all significantly exacerbated at temperatures < -20ºC and at high discharge rate, where Li^+ de-solvation in particular has been observed to dominate the capacity fade.[5] In general, these resistances have been minimized by employing low melting-point solvents[6], and novel salt additives.[7] Though much progress has been made, it is crucial to note that these advancements have been largely been applied conventional LIBs containing transition-metal oxide electrodes. These electrodes operate via the "rocking chair" mechanism, where Li^+ diffuses from negative electrode to positive electrode during discharge, undergoing solvation at the negative electrode interface and de-solvation at the positive electrode interface. As a consequence of such a mechanism, sluggish Li^+ desolvation is completely unavoidable during both charge and discharge of LIBs. This is not the case for dual-ion batteries (DIBs), however. DIBs store both cations and anions during charge, which migrate back into the electrolyte during discharge. This "salt-splitting" mechanism intrinsically decouples solvation and desolvation, where ions undergo desolvation on both electrodes during charge and solvation on both electrodes during discharge, theoretically circumventing the desolvation barrier.[8] Furthermore, the weak solvation of anions suggests that the de-solvation barrier would have little effect on the positive electrode kinetics.[9] These factors indicate that DIBs have the potential to kinetically outperform LIBs at extremely low temperature.

Anion-storing DIB positive electrodes typically fall into the following categories: anion doping in polymers[10], anion insertion in metal-organic frameworks (MOFs)[11], halogen conversion in graphite[12], and anion intercalation in graphite.[13] Polymers have recently shown promise for low temperature devices[6a,b], however the poor volumetric energy density and low electronic conductivity of polymer electrodes hinders their widespread adoption. Furthermore, halogen conversion has yet to be realized in organic electrolytes, and the unclear solvation/desolvation

mechanics at the electrode interface of polymers and MOFs overcomplicates a direct comparison between DIB and LIB mechanisms.[10-12] The well-known intercalation based graphite positive electrode is the ideal candidate to make such a comparison, however until now an electrolyte system with adequate oxidative stability and low temperature ionic conductivity has not been demonstrated.

Herein, we demonstrate the holistic design of practical dual-graphite batteries for use at extremely low temperature, utilizing a novel electrolyte that simultaneously offers high low temperature ionic conductivity and electrochemical stability. While this electrolyte provides excellent performance to LIB chemistries at low temperature, we show that a DIB full cell far exceeds the LIB control in terms of kinetics, leading to an 11 times greater capacity retention at -60 ºC at a 10 C discharge rate. These findings are further supported by impedance and GITT trends at different operating temperatures. This work offers a new mechanistic design criterion towards the development of practical low temperature batteries capable of high-power output.

Results and Discussion

Methyl propionate (MP), a common carboxylate ester was chosen as the primary solvent in our electrolyte for its sufficient dielectric constant and low melting point of -87.5 ºC (Table S1). $LiPF_6$ was selected as the salt due to the established viability of PF_6^- intercalation in graphite, and 2 M concentration was selected to satisfy the concentration requirements of DIBs without producing a high viscosity.[13] As presented in **Figure 1A**, MP-based electrolytes remain in liquid phase at -60ºC, well past the freezing point of a typical electrolyte used in commercial batteries (1 M $LiPF_6$ in ethylene carbonate/diethyl carbonate or EC/DEC, 1:1 volume). While carboxylate esters has previously been applied in low-temperature batteries, their role has been limited to an additive to

typical EC and ethyl methyl carbonate (EMC) based systems.[6c,e] We suggest that their limitation in this regard likely stems from poor reductive stability, where cyclic voltammetry (CV) of 2 M $LiPF_6$ in MP significant cathodic current beginning at 0.5 V vs. Li/Li^+, and irreversible Li plating (**Figure 1B**). To solve this issue, fluoroethylene carbonate (FEC), which is known to stabilize negative electrode and positive electrode interfaces was applied to the MP system, where 2 M $LiPF_6$ in MP with 10% (v/v) FEC (MP 10% FEC) additive shows the lowest anodic current at high voltage while enabling reversible Li plating at low voltage **(Figure 1B)**.[14] The FEC additive also serves to build a solid-electrolyte interface (SEI) capable of enabling graphite negative electrodes, which is vital to the practicality of low temperature batteries until Li metal negative electrodes can be successfully enabled at high coulombic efficiency. However, the pure MP electrolyte without FEC fails to support charge/discharge of graphite negative electrodes (**Figure 1C**). While high FEC concentrations can likely achieve this, we determined that 10% (v/v) FEC was the minimum amount required to do so (Figure S2A), which was selected to maximize the MP composition for a low overall melting point and viscosity.

The aforementioned electrolyte design principles are perhaps best exemplified in the measured ionic conductivity with decreasing temperature (**Figure 1D**). Using an incremental impedance measurement technique (Supporting Information), it was found that 2M $LiPF_6$ in MP retained a remarkable ionic conductivity of 1.89 mS cm^{-1} at -60 ºC, which was slightly reduced to 1.50 mS cm^{-1} with the addition of 10% FEC. This is in stark contrast to the commercial carbonate electrolyte, which falls to 0.0051 mS cm^{-1} at -60 ºC (**Figure 1D**).

To evaluate DIBs and LIBs at low temperature we applied the 2 M $LiPF_6$ MP 10% of FEC electrolyte in graphite||graphite and graphite||$LiCoO_2$ (LCO) full-cells. Their charge storage mechanisms are displayed in **Figure 2A&B**, respectively to illustrate the distinct

solvation/desolvation behavior. The graphite positive electrode was found to exhibit lower specific capacity of 80 mAh g^{-1} compared to the 138 mAh g^{-1} of LCO due to the greater size of PF_6^- relative to Li^+ (Figure S3). However, as displayed in **Figure 2C**, the storage of PF_6^- (~ 4.6 – 5.2 V vs. Li/Li^+) in graphite occurs at a much higher potential than Li^+ in LCO (~ 3.9 – 4.2 V vs. Li/Li^+), indicating its viability in terms of energy output. These positive electrode chemistries were then applied in full cells with graphite negative electrodes with voltage profiles shown in **Figure 2D**&**E**. The detailed design of these full cells can be found in the supporting information. The cycling performance of these cells are shown in **Figure 2F**, where stable performance was exhibited for both cells after a commonly applied initial pre-lithiation process for the DIB (Supporting Information). The capacity fading of such cycling has been recently studied by Heidrich et al., indicating that the irreversibility of the graphite positive electrode can potentially result in Li metal plating on the negative electrode.[15] While this was not explored in this work, a focus of future studies will be to address these with more stable electrolyte chemistries and optimized N/P ratios.

To simulate low temperature device operation, the assembled full-cells were then subjected to testing using a method similar to previous studies (Supporting Information).[5,6] At -40ºC with a 1 C discharge rate the graphite||LCO LIB was found to retain 72.4% of its room temperature capacity, which decreased to 63.2% at -60ºC (**Figure 3A**). It is worth noting that due to the adoption of the new electrolyte the graphite||LCO control cell ranks among the best capacity retention for this temperature, as displayed by the performance comparison in Figure S5.[6] Despite the high-performing control, the graphite||graphite DIB was found to far exceed the LIB capacity retention, retaining 93.1% and 84.4% of its room temperature capacity at -40 ºC and -60 ºC, respectively (**Figure 3B**). The low temperature improvement of the DIB mechanism was further investigated at -60ºC under different discharge rates, which provided perhaps the most salient

deviation of performance metrics (**Figure 3C&D**). At -60 ºC and a 0.1 C discharge rate, the graphite||LCO LIB and the graphite||graphite DIB displayed 78.1% and 87.3% capacity retentions, respectively. However, when the rate was increased to 10 C, the DIB still exhibited 61.7%, whereas the LIB was unable to provide any significant capacity (5.5%) under the same conditions. The room temperature capacity retention trend is displayed in Figure S6C in its entirety, and can be compared to the same trends at room temperature (Figure S6A& B), where little deviation can be observed between the two cells. These trends withstanding, DIBs typically struggle to match LIBs in specific energy at a cell level due to the higher electrolyte volume demanded (Table S2&3).[16] However, DIBs could be ideal for applications requiring high power output at extremely low temperature due to the sluggish kinetics of LIBs.[2,6]

To better understand the remarkable kinetic performance of the DIB at extremely low temperature, further electrochemical characterization was performed on the graphite and LCO positive electrodes to isolate the source of the two storage mechanisms. First, the galvanostatic intermittent titration technique (GITT) was applied to the two positive electrodes at room temperature and -60ºC (**Figure 4A&B**), a technique which has previously applied to study other positive electrodes at low temperature.[17] The data obtained from the tests were used to calculate the diffusion coefficients for Li^+ and PF_6^- in the LCO and graphite positive electrodes, respectively using a spherical particle model applied in previous literature (**Figure 4C**).[18] At 23 ºC the average diffusion coefficient was determined to be $2.5\ x\ 10^{-8}$, and $2.1\ x\ 10^{-10} cm^2\ s^{-1}$ for the graphite and LCO positive electrodes, respectively. The graphite positive electrode values vary from previous studies, which may be related to a previously established self-activation process that occurs during our GITT preparation (Supporting Information).[13a,13f,19] When the same analysis was applied at -60 ºC, these values decreased to $4.1\ x\ 10^{-10} cm^2\ s^{-1}$ and $7.6\ x\ 10^{-14} cm^2\ s^{-1}$,

where the LCO declined by almost double the orders of magnitude compared to the graphite positive electrode. Such a decrease in the LCO GITT is likely due to the combined effects of solid-state diffusion and de-solvation, whereas the graphite positive electrode only experiences the former. This trend was further investigated by electrochemical impedance spectroscopy (EIS) applied to 50 % state of charge (SOC) symmetric positive electrode cells to eliminate any contribution of the shared graphite negative electrode to the charge transfer impedance (**Figure 4D&E**). It can be observed that with decreasing temperature the graphite positive electrode exhibits consistently lower charge transfer impedance (R_{CT}) than LCO, which was measured to be 7.26 Ω and 94.1 Ω, respectively at -60 ºC (**Figure 4F**). In agreement with the GITT results, we attribute this trend to the elimination of desolvation in the anion storing positive electrodes. The summary of equivalent circuit element values can be found in Tables S4 &5.

Despite this, it is also important to note the limitations of electrochemical characterization techniques. Specifically, the EIS equivalent circuit and GITT diffusion coefficient model may be insufficient to quantitatively differentiate the effects of solid-state and desolvation effects during charge-transfer. Furthermore, the assumptions inherent in GITT such as negligible volume change, and dominant solid-state diffusion are problematic. While these factors may undermine the quantitative precision of these techniques, the qualitative comparison between the graphite and LCO positive electrodes clearly supports the performance data presented in this work, demonstrating the superiority of the DIB mechanism for low temperature applications.

Conclusion

To summarize, we demonstrated the comprehensive design of extremely low temperature batteries in order to confirm the kinetic superiority of the salt-splitting charge-transfer mechanism found in

DIBs . First, using MP as the primary solvent with a modest addition of 10% FEC, we formulated a novel electrolyte providing exceptional ionic conductivity at low temperature and high oxidative stability without compromising graphite negative electrode performance. This electrolyte was then applied in practical dual-graphite and graphite||LCO full-cells, which were subjected to testing at the extremely low temperature of -60 ºC, where the dual-graphite DIBs provided consistently greater capacity retention compared to the LIBs for moderate and high discharge rates despite being comparable in this regard at room temperature. These trends were further justified by GITT and AC impedance measurements, which measured a significantly smaller increase in the ion diffusion barrier and the charge transfer impedance for the graphite positive electrode compared to LCO when operating at -60 ºC. Looking ahead, new electrolytes in support of more stable graphite positive electrodes, novel anion-storing positive electrodes, and more precise electrochemical techniques for low temperature analysis will be vital to the development of next-generation DIBs for use at extremely low temperature.

Conflict of Interest

A patent was filed for this work through the UCSD Office of Innovation and Commercialization.

Acknowledgements

This work was partially supported by an Early Career Faculty grant from NASA's Space Technology Research Grants Program (ECF 80NSSC18K1512) to Z.C.. P.L. and Z.C. acknowledge the start-up fund from Jacob School of Engineering at UCSD. The majority of cell fabrication and electrochemical testing was performed in the UCSD-MTI Battery Fabrication and

the UCSD-Arbin Battery Testing Facility. This work was performed in part at the San Diego Nanotechnology Infrastructure (SDNI) of UCSD, a member of the National Nanotechnology Coordinated Infrastructure, which is supported by the National Science Foundation (Grant ECCS-1542148). J.H. conceived the original idea and initial experimental plan. Z.C. and P.L. directed the project. J.H. carried out the experiments. Y.Y. and M.L. assisted with characterization. J.H., Z.C., and P.L. wrote the paper. All authors discussed the results and commented on the manuscript.

Keywords: Low-temperature batteries, liquid electrolyte, dual ion battery, ion solvation, high power

10.1002/anie.201912167

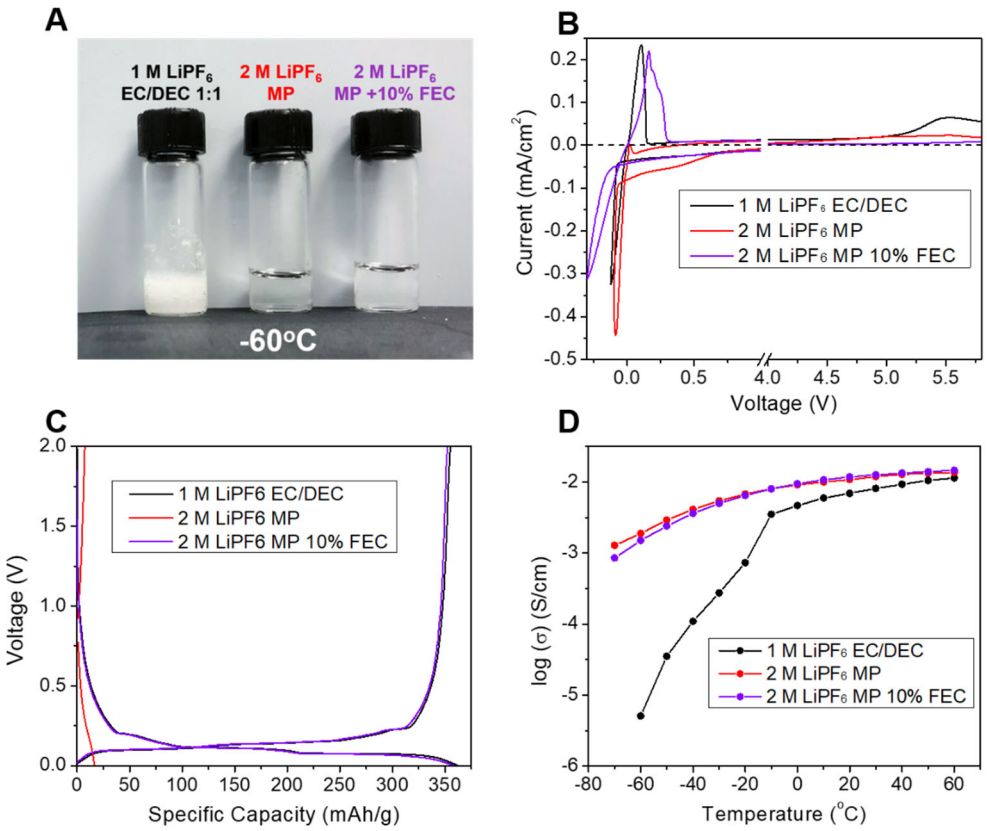

Figure 1. Electrolyte characteristics. **A)** Image of selected electrolytes at -60°C. **B)** CV profiles of stainless-steel electrodes in selected electrolytes at 1 mV s^{-1}. **C)** Half-cell charge/discharge profiles of graphite negative electrodes in selected electrolytes at 0.1 C. **D)** Ionic conductivity of selected electrolytes measured at different temperatures.

10.1002/anie.201912167

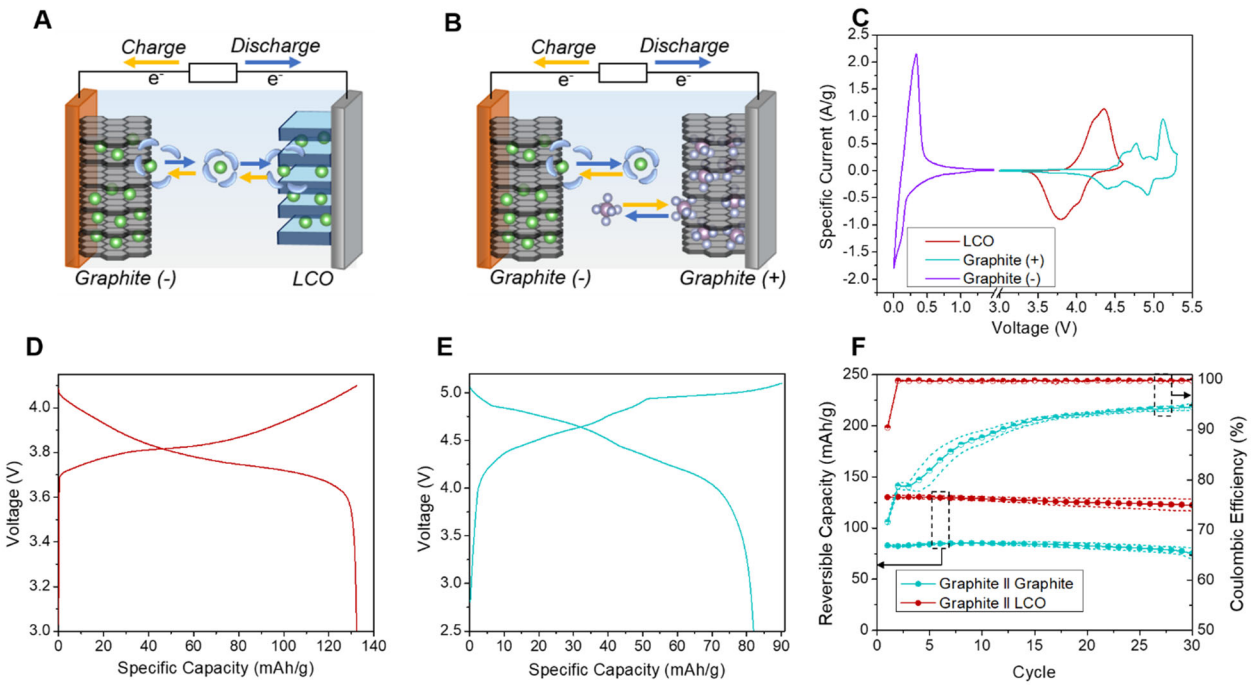

Figure 2. Operational schematics of **A)** Graphite||LCO, and **B)** Graphite||graphite full-cells. **C)** CV profiles of the selected electrode half-cells in 2 M $LiPF_6$ in MP 10% FEC at 1 mV s^{-1}. Room temperature charge/discharge profiles of **D)** Graphite||LCO and **E)** Graphite||graphite full-cells at 1C (based on 140 mAh g^{-1} and 80 mAh g^{-1}, respectively). **F)** Room temperature full-cell cycling performance at 1C. Dashed lines represent error bars.

10.1002/anie.201912167

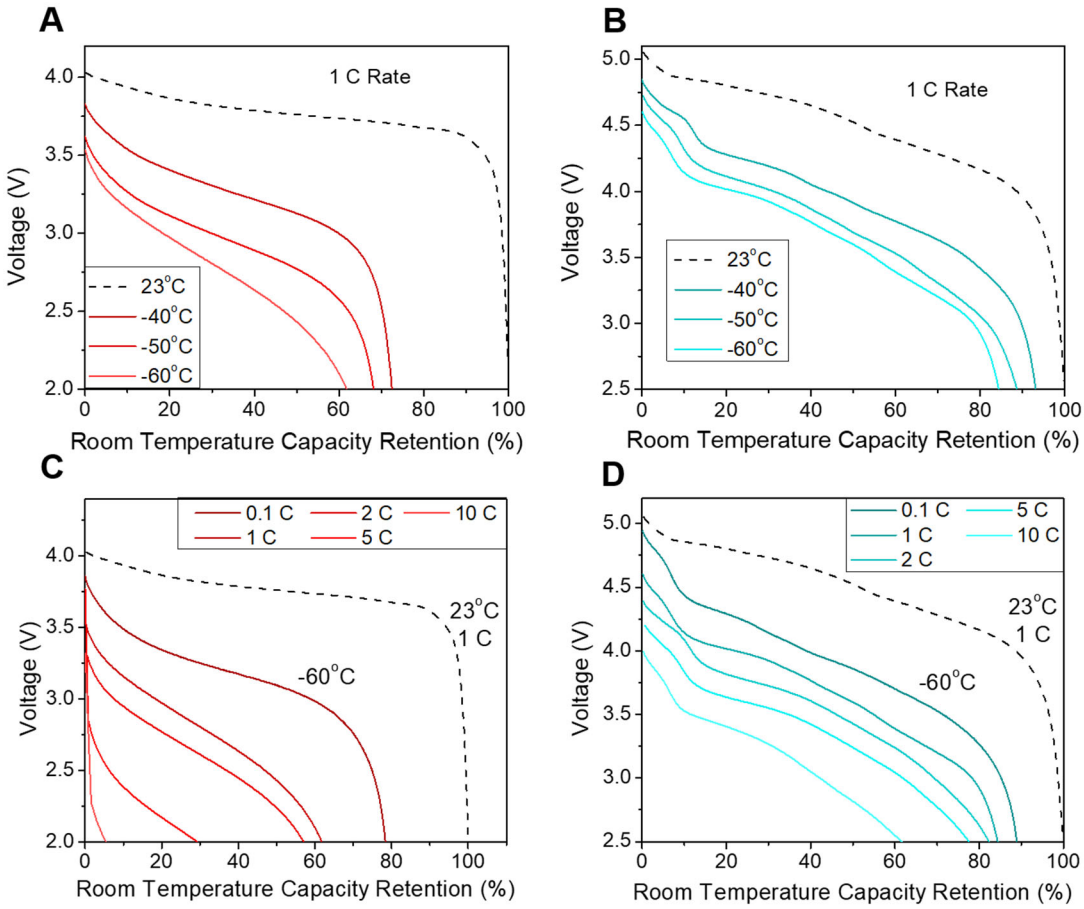

Figure 3. Discharge profiles of **A)** Graphite||LCO, and **B)** Graphite||Graphite full-cells at different temperatures and 1 C rate. -60 ºC discharge profiles of **C)** Graphite||LCO, and **D)** Graphite||graphite full-cells in 2 M $LiPF_6$ in MP 10 % FEC at different rates compared to room temperature (23ºC). Retention was based on the measured room temperature discharge capacity at 1 C.

10.1002/anie.201912167

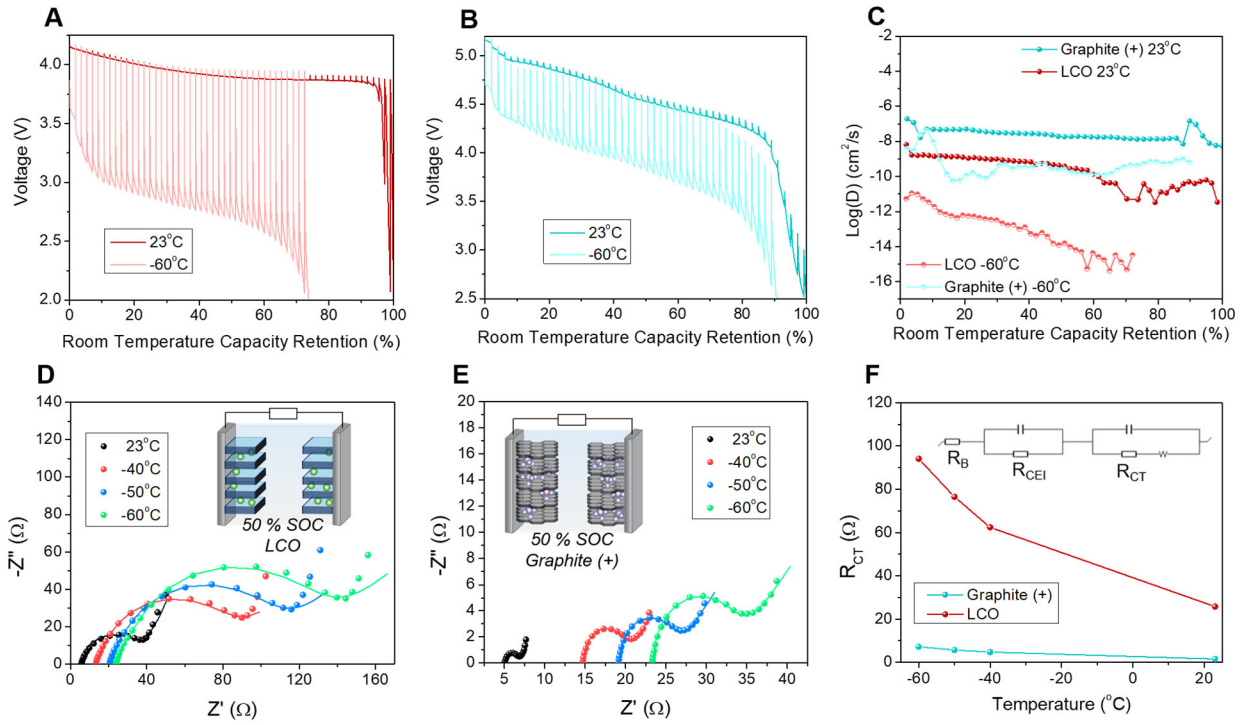

Figure 4. GITT Discharge curves of **A)** LCO and **B)** Graphite half-cells in 2 M $LiPF_6$ in MP 10 % FEC at 1 C for room temperature and -60ºC. **C)** Measured ion diffusion coefficient during discharge in the selected positive electrodes at room temperature and -60ºC. Nyquist impedance and equivalent circuit fitting of **D)** LCO||LCO and **E)** Graphite positive electrode||graphite positive electrode coin cells at various temperatures in a 50% SOC condition. **F)** Summarized charge transfer resistance vs. temperature.

10.1002/anie.201912167

Graphical Abstract

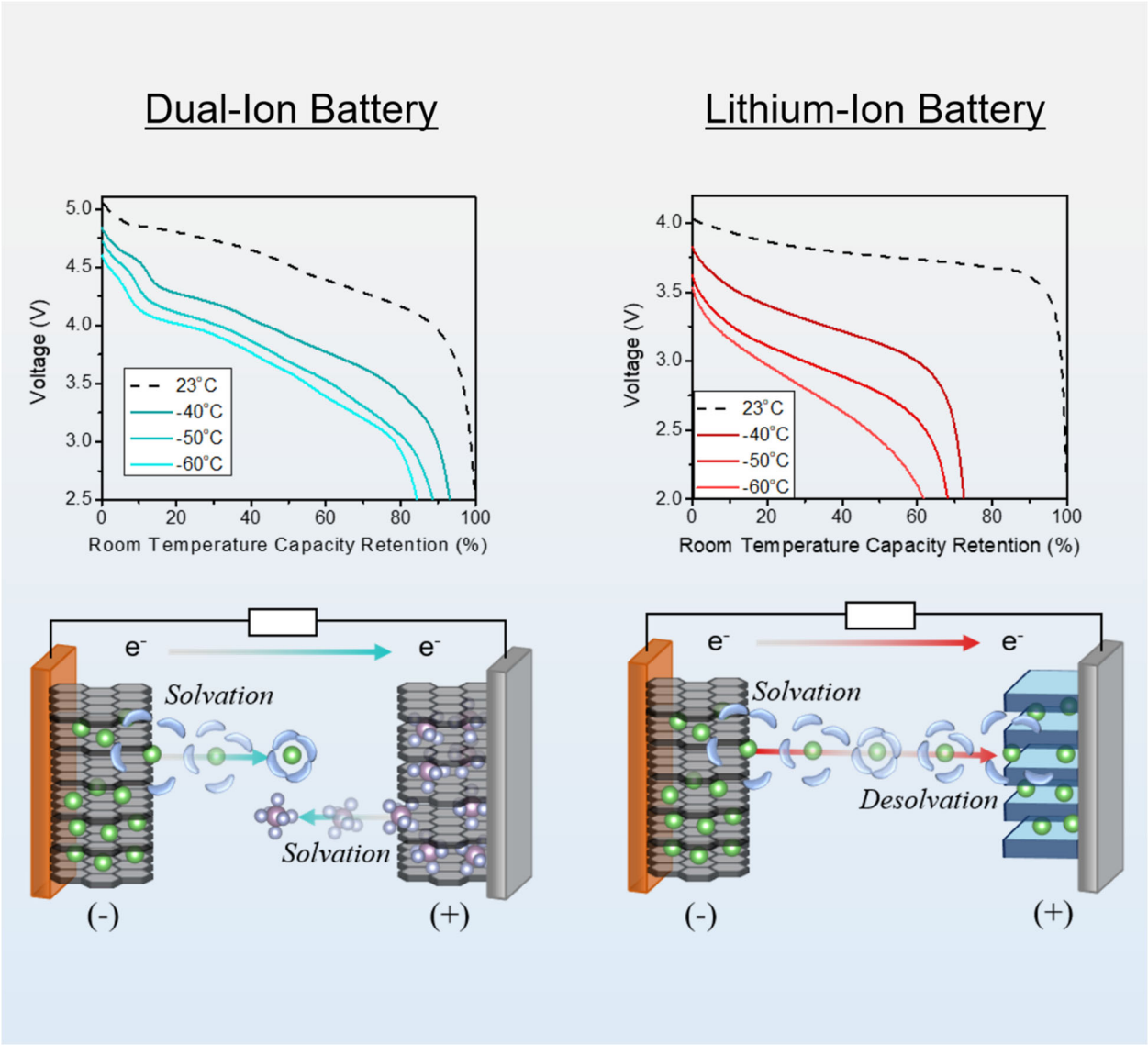

The field of low temperature batteries has been historically dominated by the study of Li-ion cells operating under the "rocking-chair" mechanism. This design choice is challenged via the rational design of "salt-splitting" dual-graphite batteries which exploit cation and anion storage mechanics to circumvent sluggish desolvation during discharge.

References

[1] a) M. Winter, B. Barnett, K. Xu, *Chem. Rev.* **2018**, *118*, 11433–11456; b) J. B. Goodenough, Y. Kim, *Chem. Mater.* **2010**, *22*, 587–603.

[2] a) M. C. Smart, B. V. Ratnakumar, R. C. Ewell, S. Surampudi, F. J. Puglia, R. Gitzendanner, *Electrochim. Acta* **2018**, *268*, 27–40; b) K. B. Chin, E. J. Brandon, R. V. Bugga, M. C. Smart, S. C. Jones, F. C. Krause, W. C. West, G. G. Bolotin, *Proc. of the IEEE* **2018**, *106*, 419–428; c) J. Jaguemont, L. Boulon, Y. Dubé, *Applied Energy* **2016**, *164*, 99–114; d) C.-K. Huang, J. S. Sakamoto, J. Wolfenstine, S. Surampudi, *J. Electrochem. Soc.* **2000**, *147*, 2893–2896; e) G. Zhu, K. Wen, W. Lv, X. Zhou, Y. Liang, F. Yang, Z. Chen, M. Zou, J. Li, Y. Zhang, et al., *J. Power Sources* **2015**, *300*, 29–40; f) S. S. Zhang, K. Xu, T. R. Jow, *Electrochim. Acta* **2002**, *48*, 241–246.

[3] G. Nagasubramanian, *J. Appl. Electrochem.* **2001**, *31*, 99–104.

[4] a) Y. Ji, C. Y. Wang, *Electrochim. Acta* **2013**, *107*, 664–674; b) C.-Y. Wang, G. Zhang, S. Ge, T. Xu, Y. Ji, X.-G. Yang, Y. Leng, *Nature* **2016**, *529*, 515–518.

[5] a) S. S. Zhang, K. Xu, T. R. Jow, *J. Power Sources* **2003**, *115*, 137–140; b) Q. Li, D. Lu, J. Zheng, S. Jiao, L. Luo, C.-M. Wang, K. Xu, J.-G. Zhang, W. Xu, *ACS Appl. Mater. Interfaces* **2017**, *9*, 42761–42768.

[6] a) X. Dong, Z. Guo, Z. Guo, Y. Wang, Y. Xia, *Joule* **2018**, *2*, 902–913; b) X. Dong, Y. Lin, P. Li, Y. Ma, J. Huang, D. Bin, Y. Wang, Y. Qi, Y. Xia, *Angew. Chem. Int. Ed.* **2019**, *58*, 5623–5627; c) M. C. Smart, B. V. Ratnakumar, K. B. Chin, L. D. Whitcanack, *J. Electrochem. Soc.* **2010**, *157*, A1361–A1374; d) C. S. Rustomji, Y. Yang, T. K. Kim, J. Mac, Y. J. Kim, E. Caldwell, H. Chung, Y. S. Meng, *Science* **2017**, eaal4263; e) M. C. Smart, B. L. Lucht, S. Dalavi, F. C. Krause, B. V. Ratnakumar, *J. Electrochem. Soc.* **2012**, *159*, A739–A751; f) M. C. Smart, B. V. Ratnakumar, L. D. Whitcanack, K. B. Chin, S. Surampudi, H. Croft, D. Tice, R. Staniewicz, *J. Power Sources* **2003**, *119–121*, 349–358; g) E. J. Plichta, M. Hendrickson, R. Thompson, G. Au, W. K. Behl, M. C. Smart, B. V. Ratnakumar, S. Surampudi, *J. Power Sources* **2001**, *94*, 160–162; h) D. Yaakov, Y. Gofer, D. Aurbach, I. C. Halalay, *J. Electrochem. Soc.* **2010**, *157*, A1383–A1391.

[7] B. Liao, H. Li, M. Xu, L. Xing, Y. Liao, X. Ren, W. Fan, L. Yu, K. Xu, W. Li, *Adv. Energy Mater.* **2018**, *8*, 1800802.

[8] a) M. Wang, Y. Tang, *Adv. Energy Mater.* **2018**, *8*, 1703320; b) X. Zhou, Q. Liu, C. Jiang, B. Ji, X. Ji, Y. Tang, H.-M. Cheng, *Angew. Chem. Int. Ed.* **2019**; c) I. A. Rodríguez-Pérez, X. Ji, *ACS Energy Lett.* **2017**, *2*, 1762–1770.

[9] a) Y. Aihara, T. Bando, H. Nakagawa, H. Yoshida, K. Hayamizu, E. Akiba, W. S. Price, *J. Electrochem. Soc.* **2004**, *151*, A119–A122; b) J. O. Bockris, A. K. N. Reddy, M. E. Gamboa-Aldeco, *Modern Electrochemistry 2A: Fundamentals of Electrodics*, Springer US, **2000**.

[10] a) S. Muench, A. Wild, C. Friebe, B. Häupler, T. Janoschka, U. S. Schubert, *Chem. Rev.* **2016**, *116*, 9438–9484; b) J. K. Feng, Y. L. Cao, X. P. Ai, H. X. Yang, *J. Power Sources* **2008**, *177*, 199–204; c) C. Su, F. Yang, L. Ji, L. Xu, C. Zhang, *J. Mater. Chem. A* **2014**, *2*, 20083–20088; d) L. Fan, Q. Liu, Z. Xu, B. Lu, *ACS Energy Lett.* **2017**, *2*, 1614–1620.

[11] a) M. L. Aubrey, J. R. Long, *J. Am. Chem. Soc.* **2015**, *137*, 13594–13602; b) S. Dühnen, R. Nölle, J. Wrogemann, M. Winter, T. Placke, *J. Electrochem. Soc.* **2019**, *166*, A5474–A5482.

[12] C. Yang, J. Chen, X. Ji, T. P. Pollard, X. Lü, C.-J. Sun, S. Hou, Q. Liu, C. Liu, T. Qing, et al., *Nature* **2019**, *569*, 245–250.

[13] a) G. Wang, M. Yu, J. Wang, D. Li, D. Tan, M. Löffler, X. Zhuang, K. Müllen, X. Feng, *Adv. Mater.* **2018**, *30*, 1800533; b) K. V. Kravchyk, P. Bhauriyal, L. Piveteau, C. P. Guntlin, B. Pathak, M. V. Kovalenko, *Nat. Commun.***2018**, *9*, 4469; c) J. A. Seel, J. R. Dahn, *J. Electrochem. Soc.* **2000**, *147*, 892–898; d) X. Zhang, Y. Tang, F. Zhang, C.-S. Lee, *Adv. Energy Mater.* **2016**, *6*, 1502588; e) T. Placke, O. Fromm, S. F. Lux, P. Bieker, S. Rothermel, H.-W. Meyer, S. Passerini, M. Winter, *J. Electrochem. Soc.* **2012**, *159*, A1755–A1765; f) S. Miyoshi, H. Nagano, T. Fukuda, T. Kurihara, M. Watanabe, S. Ida, T. Ishihara, *J. Electrochem. Soc.* **2016**, *163*, A1206–A1213; g) H. Fan, L. Qi, H. Wang, *Solid State Ionics* **2017**, *300*, 169–174; h) Y. Huang, H. Fan, H. Kamezaki, B. Kang, M. Yoshio, H. Wang, *ChemElectroChem* **2019**, *6*, 2931–2936; i) J. Lang, J. Li, F. Zhang, X. Ding, J. A. Zapien, Y. Tang, *Batteries & Supercaps* **2019**, *2*, 440–447; j) M. Wang, C. Jiang, S. Zhang, X. Song, Y. Tang, H.-M. Cheng, *Nature Chem.* **2018**, *10*, 667–672; k) C. Jiang, Y. Fang, W. Zhang, X. Song, J. Lang, L. Shi, Y. Tang, *Angew. Chem. Int. Ed.* **2018**, *57*, 16370–16374; l) S. Wang, S. Jiao, D. Tian, H.-S. Chen, H.

Jiao, J. Tu, Y. Liu, D.-N. Fang, *Adv. Mater.* **2017**, *29*, 1606349; m) Z. Zhou, N. Li, Y. Yang, H. Chen, S. Jiao, W.-L. Song, D. Fang, *Adv. Energy Mater.* **2018**, *8*, 1801439; n) Z. Yu, S. Jiao, S. Li, X. Chen, W.-L. Song, T. Teng, J. Tu, H.-S. Chen, G. Zhang, D.-N. Fang, *Adv. Funct. Mater.* **2019**, *29*, 1806799.

[14] a) H. Shin, J. Park, A. M. Sastry, W. Lu, *J. Electrochem. Soc.* **2015**, *162*, A1683–A1692; b) X. Fan, L. Chen, O. Borodin, X. Ji, J. Chen, S. Hou, T. Deng, J. Zheng, C. Yang, S.-C. Liou, et al., *Nat. Nanotech.* **2018**, *13*, 715–722; c) E. Markevich, G. Salitra, K. Fridman, R. Sharabi, G. Gershinsky, A. Garsuch, G. Semrau, M. A. Schmidt, D. Aurbach, *Langmuir* **2014**, *30*, 7414–7424; d) E. Markevich, G. Salitra, D. Aurbach, *ACS Energy Lett.* **2017**, *2*, 1337–1345; e) M. Ohtake, N. Nanbu, M. Takehara, M. Ue, Y. Sasaki, *ECS Meet. Abstr.* **2008**, *MA2008-02*, 175–175.

[15] B. Heidrich, A. Heckmann, K. Beltrop, M. Winter, T. Placke, *Energy Storage Mater.* **2019**, *21*, 414–426.

[16] a) J. Betz, G. Bieker, P. Meister, T. Placke, M. Winter, R. Schmuch, *Advanced Energy Materials* **2019,** 9, 1803170; b) T. Placke, A. Heckmann, R. Schmuch, P. Meister, K. Beltrop, M. Winter, *Joule* **2018**, *2*, 2528–2550.

[17] S. Cui, Y. Wei, T. Liu, W. Deng, Z. Hu, Y. Su, H. Li, M. Li, H. Guo, Y. Duan, et al., *Adv. Energy Mater.* **2016**, *6*, 1501309.

[18] Q. Liu, X. Su, D. Lei, Y. Qin, J. Wen, F. Guo, Y. A. Wu, Y. Rong, R. Kou, X. Xiao, et al., *Nat. Energy* **2018**, *3*, 936–943.

[19] a) M. Okubo, Y. Tanaka, H. Zhou, T. Kudo, I. Honma, *J. Phys. Chem. B* **2009**, *113*, 2840–2847; b) A. Heckmann, P. Meister, L.-Y. Kuo, M. Winter, P. Kaghazchi, T. Placke, *Electrochimica Acta* **2018**, *284*, 669–680.